Materials & Design 214 (2022) 110397

Contents lists available at ScienceDirect

Materials & Design

journal homepage: www.elsevier.com/locate/matdes

Synergistic water-driven shape memory performance and improving mechanism of grading photo-thermal curing shape memory composite

Wenxin Wang [a,*], Jing Yang [a], Wei Li [b], Yongtao Yao [c,d], Yaqian Yan [a], Wenjing Wang [a], Ning Wang [a,*], Jinsong Leng [c]

[a] State Key Laboratory of Marine Resource Utilization in South China Sea, Hainan University, Haikou 570228, China
[b] The Sixth Academy of China Aerospace Science & Industry Corporation, 65 Xinhua East Road, 010010, China
[c] Center for Composite Materials and Structures, Harbin Institute of Technology, Harbin 150080, China
[d] National Key Laboratory of Science and Technology on Advanced Composites in Special Environments, Harbin Institute of Technology, Harbin 150080, China

HIGHLIGHTS

- Synergistic water-driven shape memory composite is prepared via grading photo-thermal curing method.
- Shape memory performance is improved after immersed in 0.1 mol/L HCl solution.
- The synergistic plastifications between C-F and oxygen-containing functional groups of the composites.
- Practical approach to realize the intellectualization of underwater deployment and release structure.

GRAPHICAL ABSTRACT

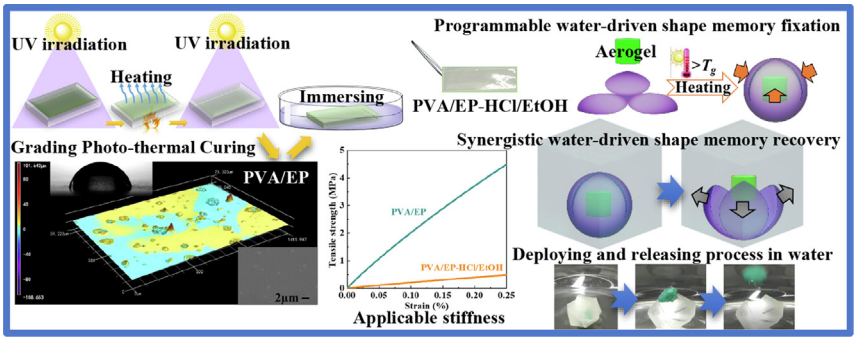

ARTICLE INFO

Article history:
Received 26 August 2021
Revised 29 December 2021
Accepted 8 January 2022
Available online 11 January 2022

Keywords:
Shape memory polymer
Synergistic water-driven
Grading photo-thermal curing
Composite
Deployment and release structure

ABSTRACT

Shape memory materials draw much attention due to various promising potential applications. This work prepares a novel shape memory composite via grading photo-thermal curing method, which has not yet been reported. Expectedly, it merges advantages of epoxy-based shape memory polymer (EP) and polyvinyl alcohol-based shape memory polymer (PVA), which has applicable stiffness and multi-stimuli responsive performance. The unsatisfactory mechanical properties of most water-driven shape memory polymer (SMP) is expected to be solved by this fabrication strategy, so that the application range of water-driven SMP could be further extended. The synergistic plasticization of PVA and EP dominates water-driven shape memory behavior of this composite. Interestingly, its water-driven shape memory performance is able to be further improved by immersed in HCl/EtOH solution. The glassy-to-rubbery modulus ratio (E'_g/E'_r) of the PVA/EP-HCl/EtOH is about 650 after immersed in 0.1 mol/L HCl/EtOH for 6 h. In addition, this immersed method also can solve the post curing problem of such cationic photocuring. It is an easy, efficient, economical strategy for improving synergistic water-driven shape memory performance. Furthermore, this shape memory composite is expected to provide new perspective and practical approach to realize the intellectualization of underwater deployment and release structure.

1. Introduction

Shape memory materials have been widely applied in aerospace, electronics, medicine, architecture, packaging, and intelli-

* Corresponding authors.
E-mail addresses: wangwenxin.999@163.com (W. Wang), wangn02@foxmail.com (N. Wang).

https://doi.org/10.1016/j.matdes.2022.110397
0264-1275/

gent structure [1,2]. As an emerging shape memory material, the SMP possesses the advantages of lightweight, large deformation, various driven modes, easy processing, simple processing, and low energy consumption [3–9]. SMP can respond sensitively to external stimulus such as heat, water, light, electricity, magnetism, infrared [9–18]. In general, their shape memory effects (SME) mainly depend on the interaction of the fixed phase and the reversible phase [19,20]. When SMP are heated to over transition temperature, the reversible phase is high elastic state. They can be programmed into temporary shape under external force with the temperature gradually reduced. When they are driven by external stimulus, the stored strain is released with recovering to the original shape [21–26].

In recent decades, researchers have studied various SMP, including epoxy-based, cyanate-based, styrene-based, and polyimide-based SMP [2,15,27,28]. Epoxy-based SMP are favored by researchers due to its mechanical properties, electrical insulation, high temperature resistance, abundant active groups and polar groups. They are usually prepared from epoxy resin, crosslinking agent, and other fillers [15,25]. The epoxy resin refers to a polymer containing two or more epoxy groups with aliphatic, alicyclic, or aromatic segments as the main chain. Herein, the ternary ring of EP composes of oxygen and carbon in the epoxy resin molecule. The charge distribution of the epoxy ring is inclined to oxygen, which increases the reactivity of the structure. Under certain conditions, the ring opening reaction easily generates with the charge transfer. During curing process of EP, their three-dimensional cross-linked network structure depends on the interaction of the main chain and active groups. Therefore, some researchers use flexible curing agent to adjust the crosslinking degree, glass transition temperature (T_g) and shape memory performance of EP [28,29]. According to different curing methods, EP can be divided into heat curing type and light curing type. The common heat curing methods usually causes some environmental pollution problems. The light curing EP mainly composes of epoxy, unsaturated monomer, curing agent, and photo-initiator. The light curing method is environmentally friendly, but it exists weakness of incomplete curing [31]. Hence, the development of a new curing process is desirable. Most driven studies of EP focus on thermal-driven method, but the report about water-driven EP is very few [15,25,29,30]. Our previous work proposed an original fabrication strategy for constructing water-driven EP, which was designed based on the chemical interaction and triggered by plasticization [15].

Recently, there are many reports about SMP with solution-driven SME and humidity sensitive SME [8,14,15,18,19,32]. Polyurethane-based SMP and gel-based SMP are relatively common [33–35]. Huang et al. first reported a polyurethane-based SMP with water-driven SME [33]. The water molecules can form strong hydrogen bond with the polar functional group C═O of polyurethane, while the hydrogen bonds between functional groups N—H and C═O of polyurethane are weakened by plasticization with the decrease of the transition temperature. PVA have a large number of hydroxyl groups, so they also are typical water-driven SMP [14,36]. In PVA, crystallized regions and hydrogen bonds work as the fixed phase, while amorphous regions work as the reversible phase. The PVA also can be used as hydrophilic functional phase to construct water-driven shape memory composites. Qin et al. prepared a PVA/ graphene oxide (GO) nanocomposite [14]. The two-dimensional GO enhance the mechanical properties of the PVA. In water, the water molecules destroy the intermolecular hydrogen bond between oxygen-containing functional groups of GO and PVA triggering water-driven SME. However, the mechanical properties of most water-driven SMP are unsatisfactory, that limit the scope of applications.

In this work, an original PVA/EP composite is proposed and designed based on previous work [15]. As shown in Scheme 1, this design strategy combines advantages of EP and PVA by grading photo-thermal curing. Interestingly, the epoxy part plays a critical role in maintaining suitable mechanical properties during water-driven SME process, and the PVA part works as prime water-driven functional phase. Therefore, the PVA/EP composite has synergistic water-driven shape memory performance. The EP and PVA part are respectively cross-linked with cationic monomer and glutaraldehyde by grading photo-thermal curing process [37]. The grading photo-thermal curing and immersing way is more saved energy and environmentally friendly than usual heat curing method, as well as solves the post curing problem. Promisingly, this composite has potential application in controlled deployment and release structure as shown in Scheme 1 (b). The pre-deformed PVA/EP-HCl/EtOH composite can wrap aerogel with temperature and external force control. The bud structure is able to deploy and release the aerogel in the water, which is controlled by programmable water-driven shape memory process.

2. Materials and methods

2.1. Materials

Epoxy resin (E-51) is purchased from Kunshan Jiulimei Electronic Material Co., Ltd. 4-thiophenyl phenyl diphenyl sulfonium hexafluoroantimonate (PC) is used as cationic photoinitiator. 3-ethyl-3-hydroxymethyl oxetane (OXT) (HPLC > 99.00%) is used as cationic monomer. They are purchased from Changzhou Tronly New Electronic Materials Co., Ltd. The cationic photoinitiator is used to generate the Lewis acid that can initiate the cationic ring-opening polymerization. PVA (alcoholysis degree: 87%-89%) and glutaraldehyde (GA) (AR, 50%) are purchased from Shanghai Aladdin Biochemical Technology Co., Ltd.

2.2. Preparation of the PVA/EP

The cationic photoinitiator (5 wt%) is mixed with E-51 (92 wt%) and cationic monomer (8 wt%). Then it is mixed with PVA precursor solution (5 vol% GA) by different proportion. This PVA/EP emulsion is poured into the mold and cured by grading photo-thermal curing method. The key parameters of this method are the time of UV irradiation and heating temperature. The PVA/EP composites with different PVA content is designated as EP (0 wt% PVA), P10 (10 wt% PVA), P30 (30 wt% PVA), P50 (50 wt% PVA), PVA (100 wt % PVA), respectively.

2.3. Characterization

The Fourier transform infrared spectroscopy (FTIR) is carried out by FTIR Spectrometer (Perkin Elmer Spectrum 100, America). X-ray diffraction (XRD) patterns of the samples are measured using XRD measurement system with 30 kV, 20 mA, and CuKα radiation (λ = 0.154 nm) (Bruker D8 Advance, Germany). The electron binding energy is measured using X-ray photoelectron spectroscopy (XPS) measurement system (Thermo Fisher Scientific ESCALAB 250Xi, America). The microscopic surface morphology is viewed with scanning electron microscope (SEM) (Hitachi S-4800, Japan). Before the test, the samples are immersed in 10 wt% KOH solution at 60 °C for 8 h and then washed with deionized water. These samples are observed by SEM after drying at 60 °C for 12 h. The mixing uniformity and surface roughness are observed by laser microscope (Keyence VK-X250K, Japan). The surface hydrophilicity is detected by contact angle meter (Powereach JC2000D4, China). Thermogravimetric analyses (TGA) are carried out with thermo-

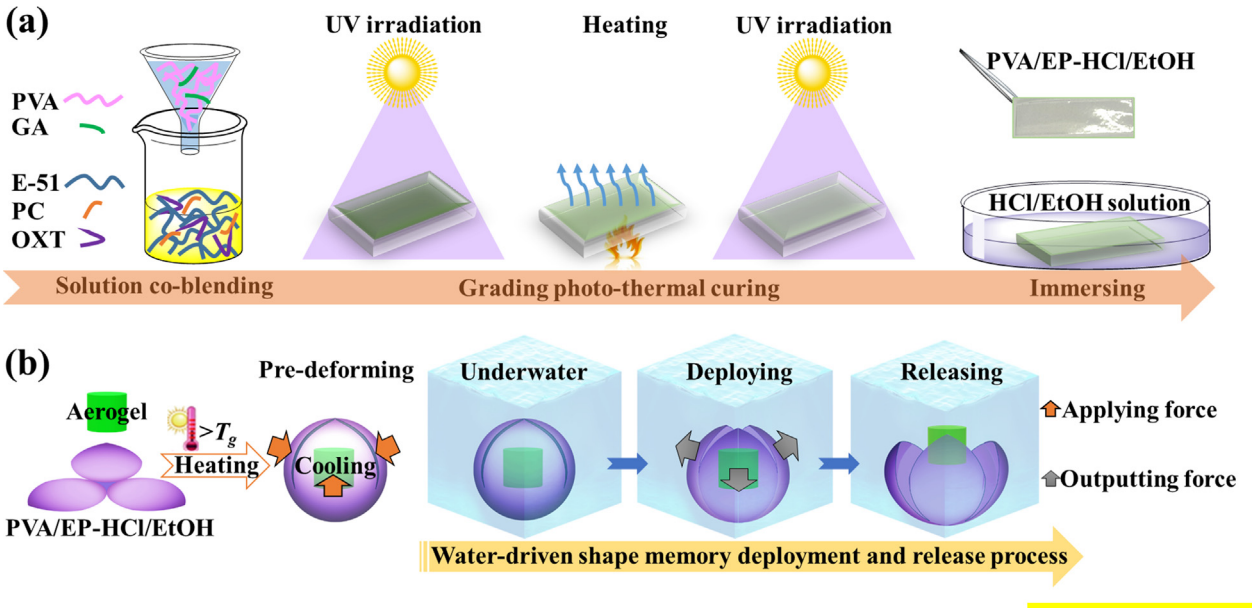

Scheme 1. The preparing process of the PVA/EP-HCl/EtOH composite (a) and the illustration of water-driven shape memory deployment and release process (b).

gravimetric analyzer (TA Instruments Q500, America) from ambient temperature to 900 °C at heating rate of 10 °C min^{-1} in nitrogen atmosphere (30 mL min^{-1}). Differential scanning calorimetry (DSC) is used to study the denaturation of the samples at heating and cooling rate of 10 °C min^{-1} in nitrogen atmosphere (TA Instruments DSC Q100, America). Dynamic mechanical analysis (DMA) is performed by DMA system (TA Instruments Q850, America) with film clamp. Rectangular samples with specimen size of 6.6 mm in width, 30 mm in length, and 0.7 mm in thickness are used at heating rate of 3 °C min^{-1} with a constant frequency of 1.0 Hz. The tan δ peaks of those samples define the T_g.

2.4. Swelling behavior

In this experiment, the simple calculation formula of swelling ratio is used to evaluate the swelling behavior of the samples. And the swelling ratio was compared by immersed in deionized water and water ethanol mixtures, respectively. Firstly, the sample was dried at 60 °C for 12 h and weighed that defined as initial weigh W_i. Secondly, it was immersed in designated solution for a certain time, and then weighed that defined as W_t. Thirdly, it was circularly immersed and weighed in certain time interval until its weight without obvious change. Its swelling ratio (W_{sr}) was calculated according Eq. (1).

$$W_{sr} = (W_t - W_i)/W_i \tag{1}$$

2.5. Shape memory behavior

Shape fixing ratio (R_f) and shape recovering ratio (R_r) are important shape memory parameters [15,16]. The test sample size is 40 mm × 3 mm × 0.5 mm. Firstly, the original state of sample is defined as initial angle (θ_o). The sample is bent into a U shape above T_g in oven. Then it is cooled to room temperature with certain external force to keep the U shape. At this time, the angle is recorded as fixed angle (θ_f). The shape memory behavior is compared in different environmental circumstances and recorded by video. The sample with fixed temporary shape is placed in a petri dish filled with deionized water at room temperature. At the same time, other deformed sample is put in a petri dish without water at room temperature. When the sample recovered to the maximum angle, the angle is recorded as recovered angle (θ_r) and the recovery time is recorded as recovered time (t_r). The θ_r is read from protractor values between the straight ends of the bent sample at the petri dish bottom. The sample is tested 5 times to reduce the experimental error. Then Eqs. (2) and (3) are used to calculate R_f and R_r of the sample.

$$R_f(\%) = \theta_f/\theta_0 \tag{2}$$

$$R_r(\%) = \theta_r/\theta_0 \tag{3}$$

3. Results and discussion

3.1. Chemical and thermodynamic properties

The differences in the molecular structure of the composites are investigated using FTIR spectrometer at the wavenumber range of 4000 cm^{-1}–650 cm^{-1}. The PVA crosslinked with 5 vol% GA is designated as PVA/GA. The molecular structures of pure PVA and PVA/GA are dramatically different in Fig. 1 (a). As is known to all, the carbonyl group is a strong polar group, in which its carbon shows positive charge, so it is easy to react with nucleophiles. On the hydroxyl group of PVA, the oxygen has lone-pair electron, which has strong nucleophilicity, so the lone-pair electron can attack the carbonyl carbon to form hemiacetal. The hydroxyl group of hemiacetal is unstable, so it is easy to dehydrate with another hydroxyl group of PVA to form acetal. Compared with the pure PVA, the C—O—C stretching vibration at 1235 cm^{-1} and the O—H peak at 3316 cm^{-1} are weakened after adding GA. The peak at 1198 cm^{-1} suggests the presence of the C—O groups in PVA/GA curing at 25 °C and 60 °C, which are different from PVA curing at 25 °C and 60 °C and highlighted with the orange circles in Fig. 1 (a). In addition, the $\sigma_{C\text{-}H}$ at 957 cm^{-1} and $\sigma_{C\text{-}H}$ at 914 cm^{-1} appear alternately. The C—H stretching vibration at the range of 3000–2793 cm^{-1} on the main chain of polyvinyl alcohol has no obvious changes. The acetal reaction requires acid catalysis and is reversible. Therefore, the C═O stretching vibration of carboxyl group at 1725 cm^{-1} and the C═O stretching vibration at 1725 $cm^{-1}$of the

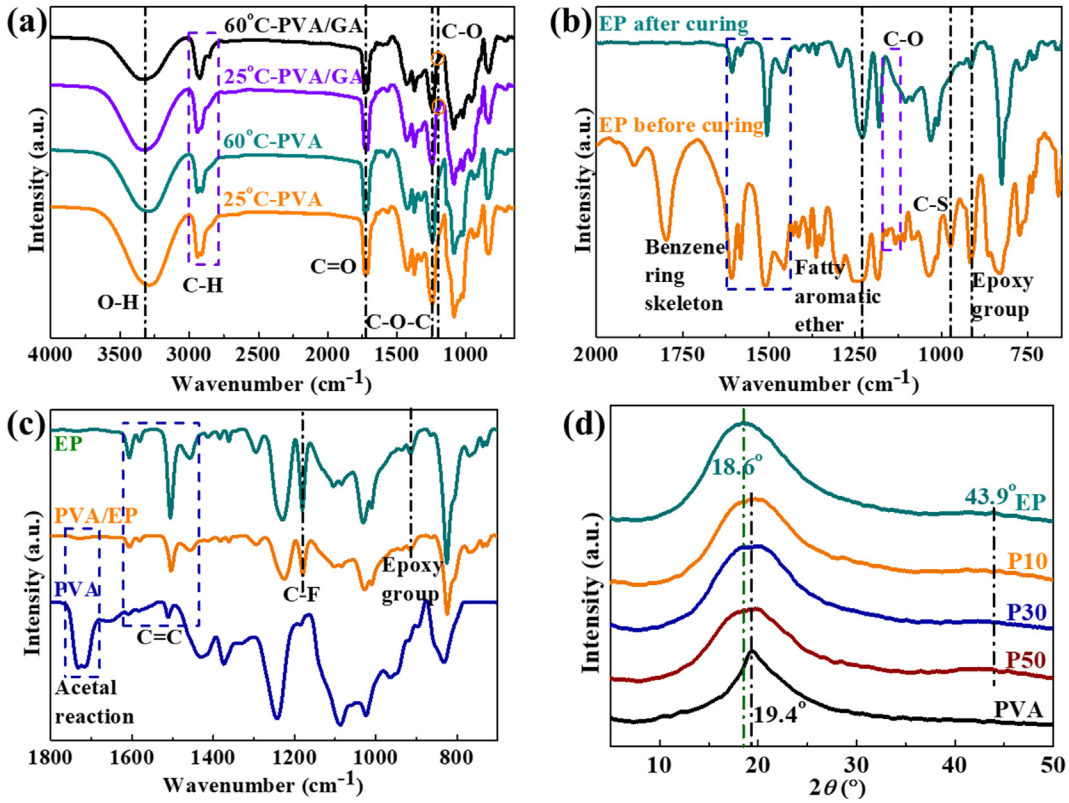

Fig. 1. FTIR spectra of PVA and PVA/GA curing at 25 °C or 60 °C (a); EP before and after curing (b); EP, the PVA/EP composite, and PVA (c); XRD patterns of EP, the PVA/EP composites, and PVA (d).

aldehyde group are attributed to the acetic acid for adjusting pH value and residual GA, respectively.

The FTIR spectra of EP before and after curing are shown in Fig. 1 (b) and Fig. S1 (a). The absorption peaks at 3180–2810 cm^{-1} and 1609–1445 cm^{-1} are the C—H stretching vibration of aliphatic chain and the C=C stretching vibration of benzene ring skeleton, respectively. When E-51 and OXT are mixed, intermolecular hydrogen bond at 3490 cm^{-1} is generated. After light curing, the E-51 undergoes the ring-opening reaction. The absorption peak at 3490 cm^{-1} disappears, which suggests the intermolecular hydrogen bond is broken. To some extent, the relative strength of epoxy group characteristic absorption peak at 912 cm^{-1} could indicate the curing degree of the EP. As the curing degree of the EP becomes higher with stronger crosslinking network, the relative strength of epoxy group characteristic absorption peak becomes weaker. The intensity of the absorption peak of the fatty aromatic ether at 1233 cm^{-1} gradually becomes strong. The C—O absorption peaks at 1159 cm^{-1} and 1135 cm^{-1} disappear due to the ring-opening reaction of the cationic monomer OXT. The C—S absorption peaks at 975 cm^{-1} disappears, which suggests the benzene ring on the cationic photo-initiator PC falls off during the light curing.

The changes in the molecular structure of the composites are shown in Fig. 1 (c) and Fig. S1 (b). Interestingly, the characteristic absorption peak at 1181 cm^{-1} indicates that the C—F is formed by F of PC and C of E-51. The absorption peak at 3322 cm^{-1} is attributed to the O—H of PVA (Fig. S1 (b)). In addition, the changes of absorption peaks at 1736 cm^{-1} and 1714 cm^{-1} provide evidences for the acetal reaction between PVA and GA. The characteristic absorption peaks at 1603 cm^{-1}, 1579 cm^{-1}, 1507 cm^{-1}, and 1456 cm^{-1} are assigned to the C=C on benzene ring skeleton of EP. The characteristic absorption peaks of EP are more obvious than the characteristic absorption peaks of PVA, so the functional groups of EP may play a major role in the performance of the PVA/EP composite. The XRD pattern of EP shows obvious amorphous property in Fig. 1 (d). There is only broad diffraction peak at 18.6°. The PVA shows [101] crystal plane diffraction peak at 19.4° [38]. Comparing with the diffraction peak of EP and PVA, the change of the PVA/EP composites diffraction peak suggests the microcrystalline regions may be formed.

The information of element composition, chemical state, and chemical bond of the various samples are obtained by the wide survey and the high-resolution XPS spectra. The C—C bond and the C—O group is basic structure of these samples, as shown in Fig. 2. The C—O is easy to form intermolecular hydrogen bond between EP and PVA. The EP and the PVA/EP composite contain the C—F bond which is corresponding to the result of FTIR spectra (1181 cm^{-1}). Predictably, the hydrogen bonding between F and water molecules will be one of influence factors on water-driven SME of the PVA/EP composites. The high-resolution XPS spectra of the C1s region for the PVA/EP composite with 10 wt% PVA is shown in Fig. 2 (c). As shown in Fig. 2 (b), (c), and (d), there is no apparent peak at 286 eV and 289 eV due to low content of PVA in this composite and low relative peak intensity of C—OH and O—C=O bonding in PVA. In Fig. 2 (d), there is O—C=O of PVA at 289 eV which is also corresponding to the analysis of FTIR spectra.

The thermodynamic properties of the samples are shown in Fig. 3 and Fig. S2. Below 85.27 °C, the weight loss of PVA can be attributed to the evaporation of entrapped water molecules. In the temperature range of 200–400 °C (313.01 °C), the hydrogen bond between PVA molecules breaks and a large number of hydroxyl groups break off from the main chain of PVA. The remaining main chain of PVA degrades during 400–800 °C (422.18 °C). For the PVA/EP composites, the tightness of their structure is affected by PVA, so their decomposition temperature is lower than EP (Fig. 3 (a)). Meanwhile, the weight loss of the PVA/EP composites

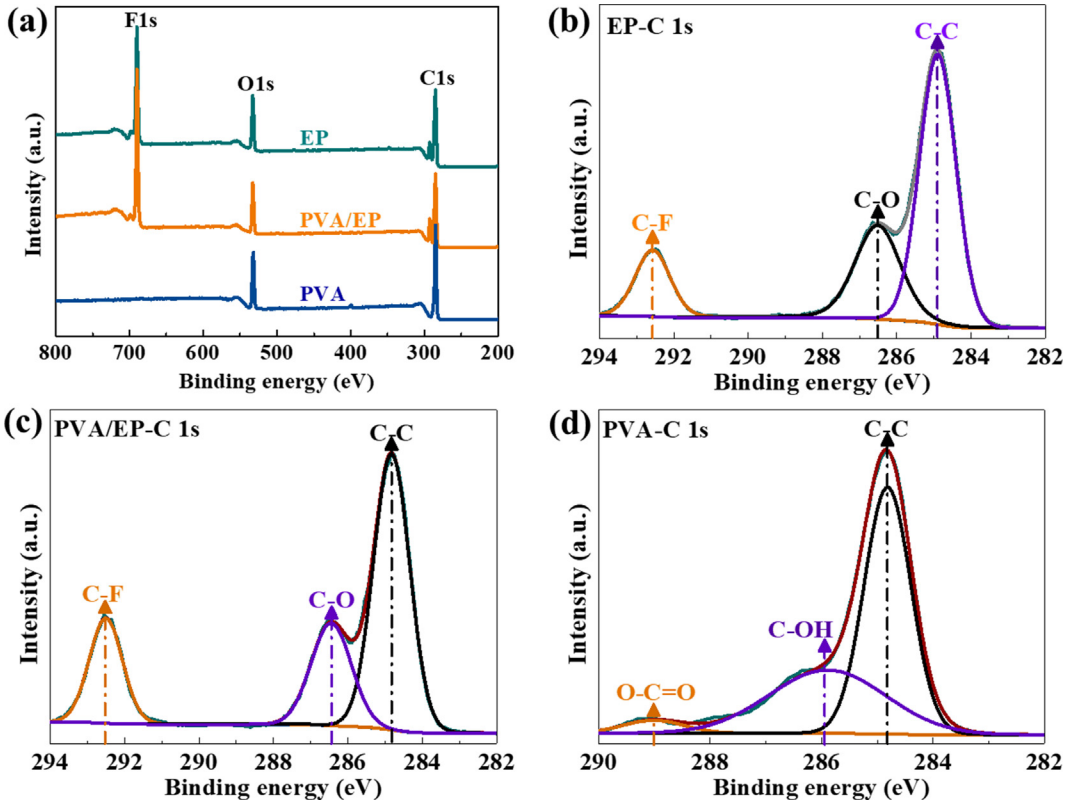

Fig. 2. Wide survey XPS spectra of EP, the PVA/EP composite, and PVA (a); high-resolution XPS spectra of the C1s region for EP (b); the PVA/EP composite (c); and PVA (d).

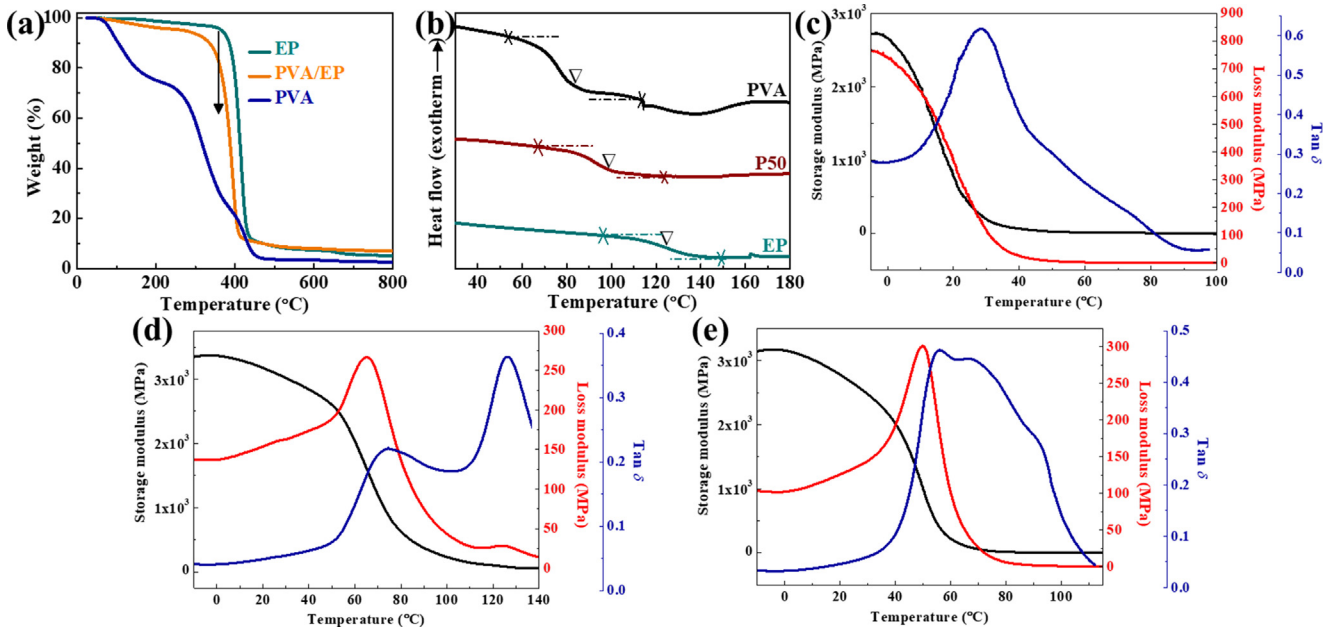

Fig. 3. TGA curves of EP, the PVA/EP composite, and PVA (a); DSC curves of EP, P50, and PVA (b); DMA thermograms of PVA (c), EP (d), and the PVA/EP composite (e).

at about 410 °C is mainly attributed to the degradation of EP. It's obvious that the PVA/EP composites also have applicable thermal stability as EP.

The T_g is an important parameter for regulating the SME performance of the SMP, which is affected by the crosslinking density, the chain segment type, and the interaction between the chain segments [14,15]. Compared with EP, the T_g of PVA is in the lower temperature range. The EP is polymerized by a cationic mechanism, so its curing rate is relatively slow and its cationic polymerization will continue after stopping the UV irradiation. Therefore, there are two tan δ peak in the DMA thermograms of EP. The T_g of the PVA/EP composites is between EP and PVA, which indicates that the addition of PVA impacts the chain segments interaction and the crosslinking structure of the composites. The DMA thermo-

grams of the PVA/EP composite after post-treatment shall analyze further on in the 3.4 section. Generally, the E'_g/E'_r is applied to roughly evaluate the SME performance of thermoset SMP, which is above 100 implying that the thermoset SMP has good SME performance. As shown in Fig. 3 (e), the E'_g/E'_r of the PVA/EP composite is above 650 indicating that it has great potential in SME performance.

3.2. Surface micromorphology and characters

Surface roughness is an important parameter that can affect fatigue strength, corrosion resistance, and swelling of the material. To a certain degree, delamination and accumulation on the surface of the composite can reflect the mixing uniformity.

The surface morphology and surface roughness parameters are obtained by laser microscope in Fig. 4 and Fig. S3. The surface arithmetic mean height (Sa) is commonly used to express the surface roughness of the material, which increases with the increasing of its surface roughness. As shown in Fig. 4 (d), the Sa of the PVA/EP composites presents a trend of gradual increase, which may be related to the difference between EP and PVA in the curing process. The EP is forming a semi-cured film under light, then the PVA will crosslink with GA while the water contained gradually evaporate to damage the composite film surfaces forming bulges or depressions, and resulting in roughened surface in the heating process. In second illumination, the uncured EP and PC continue to crosslinking. These suggest that the surface morphology and surface roughness parameters of the PVA/EP composites can be adjusted by its PVA content. In the PVA/EP composites, the PVA improve its hydrophilicity to a certain extent (Fig. 4), so the water molecules can wet the composites surface then soak into its interior.

The swelling behavior of EP, PVA, and the PVA/EP composites is observed clearly in Fig. S4. The swelling ratio of PVA shows an upward trend with immersion time increases. In immersion test, the PVA/EP composites with no obvious variation show that the composites are relative stable. In the swelling stage, the molecular movement speed of the different solvent has the large difference, the swelling speed of PVA in the water is faster than in the water/ethanol. At 100 min, the swelling ratio of PVA is about 400% in the water and only 18% in the ethanol. The solvent molecules can penetrate into the structure of their micro-crosslink net followed by physical and/or chemical interaction until equilibrium. Meanwhile, the hydrogen bonds between the functional groups of the PVA/EP composites are weakened by the solvent molecules. This plasticizing effect could play a key role in water-driven SME at a lower temperature condition.

3.3. Shape memory performance

The thermally-driven shape memory cycle of the PVA/EP composite is recorded by video and shown in Fig. 5 (a). The PVA/EP composite is configured as a flat straight strip which is the initial shape in the shape memory test. The U shape is its temporary shape. The sample with fixed temporary shape absorbs heat from thermal environment with storing heat ($T > T_g$), therefore, its shape recovering speed is relatively slow in the first 6 s. Then, its shape recovering speed gradually increases. The PVA/EP composite recovers its original state that is a flat straight strip within 28 s.

The Fig. 5 (b) shows shape memory recovery process of the EP and the PVA/EP composite in the water and in the air at room temperature. The EP and the PVA/EP composite have no obvious change both in the water and in the air for the first 6 h. The R_r of the PVA/EP composite reaches 50% in the water and is only 0% in the air at room temperature within 1 day. It indicates that the water is essential condition for inducing the shape memory recovery process of the PVA/EP composite at room temperature. The EP in the water and in the air hasn't been changed after 1 week. It is clear that the PVA/EP composite has water-driven SME and the EP hasn't. The swelling ratio of PVA/EP composites is very low (Fig. S4), so the physical swelling effect isn't the main influence for its water-driven SME. Compared with the EP and the PVA/EP composite, the PVA in the PVA/EP composite has a large number of hydrophilic hydroxyl groups which are easy to form hydrogen

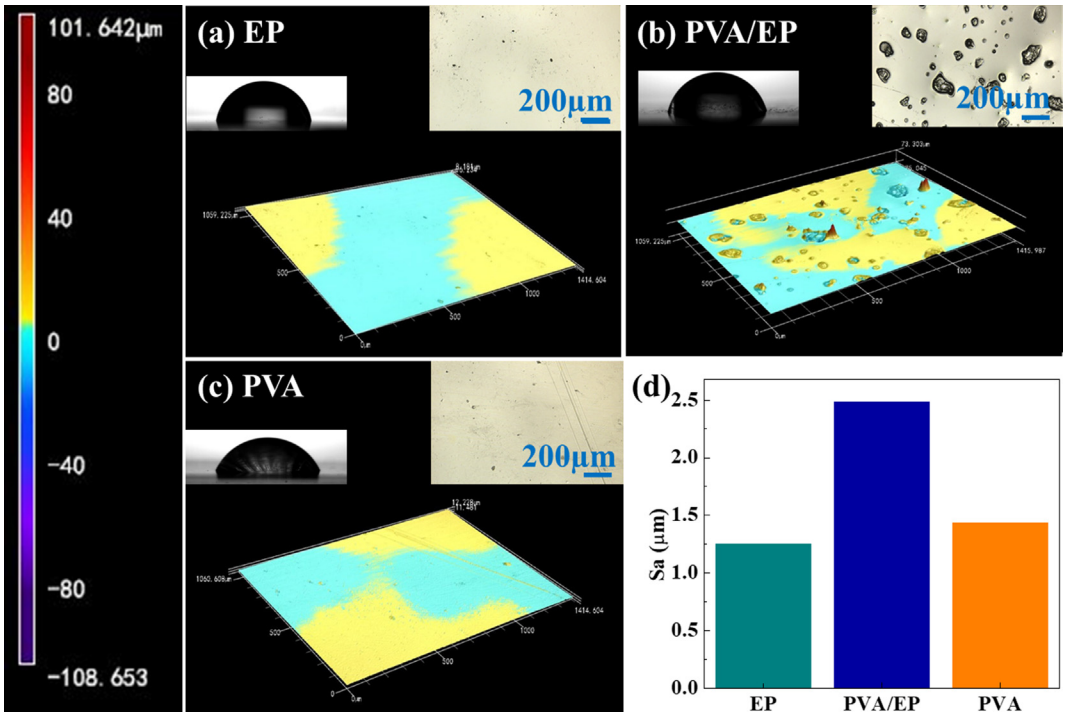

Fig. 4. Laser micrographs and contact angle photos (a ~ c) and the surface arithmetic mean height of EP, the PVA/EP composite, and PVA (d).

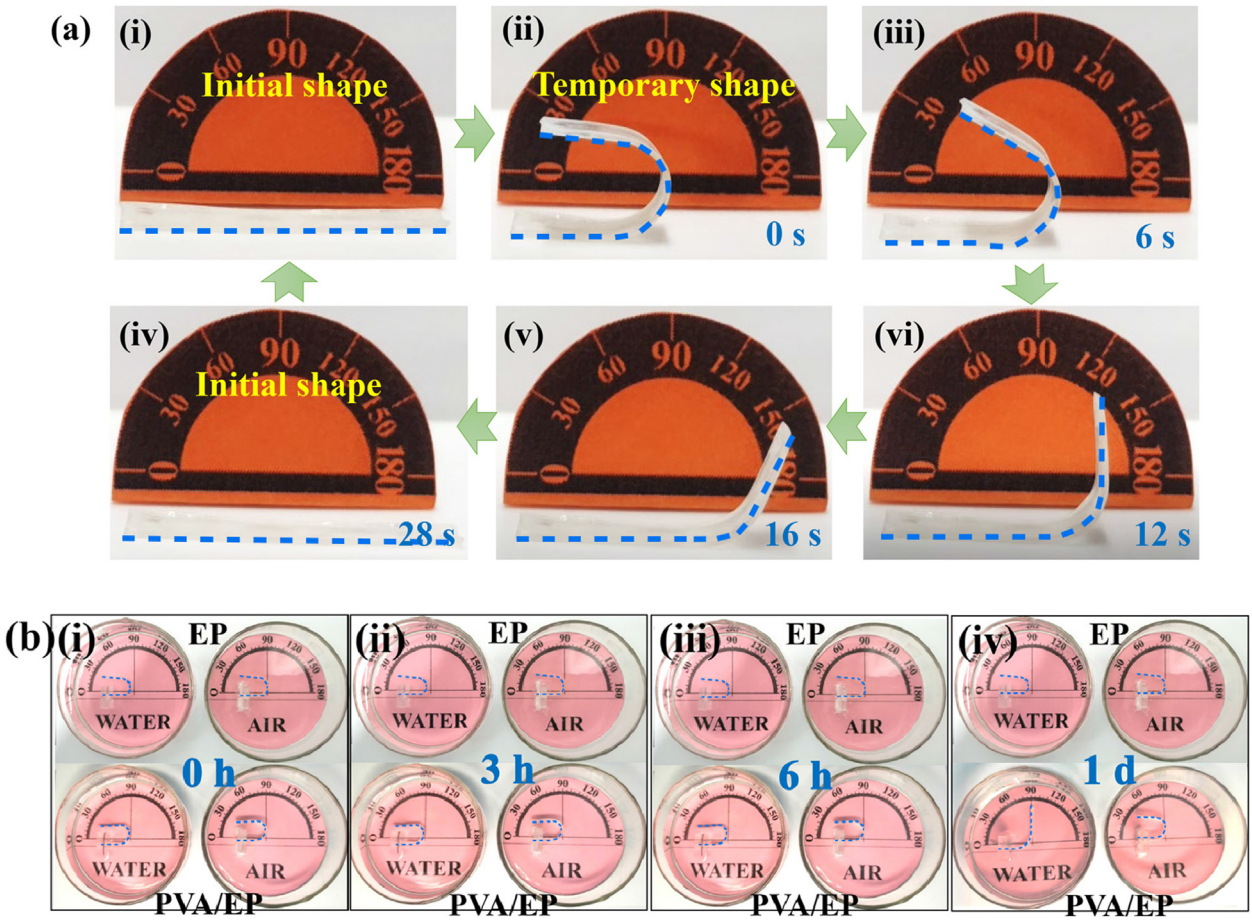

Fig. 5. Shape memory behavior. The thermally-driven shape memory cycle of the PVA/EP composite (a). Compared with shape memory recovery process of EP and the PVA/EP composite in the water and in the air at room temperature (b). In each photograph of the Fig. 5 (b): the top left corner one is EP in water; the top right corner one is EP in air; the lower left corner one is the PVA/EP composite in water; and the lower right corner one is the PVA/EP composite in air. The initial shape is a flat straight strip and the temporary shape is U shape in the shape memory test.

bonds with water molecules in humid environment, resulting in the change of aggregation structure of PVA. The water molecules can improve flexibility and mobility of the chain segment and decrease the T_g inducing its shape memory recovery process in the water at room temperature [8,14,15,18,19,32]. Moreover, the F in the PVA/EP composite also could easily form hydrogen bonds with water molecules (Fig. 2 (a)), which accelerates its water-driven shape memory recovery. Both hydroxyl groups of PVA and C-F of EP in the PVA/EP composite are important influence factors on its water-driven SME. As shown in Fig. 5 (b), the PVA/EP composite with 10 wt% PVA has water-driven SME, nevertheless, incipient slow shape memory recovering rate. The water-driven shape memory recovering speed of the composite increases with PVA content increasing in Table S1. The PVA/EP composite with 90 wt % PVA is able to recover its initial shape within 30 min. With PVA content increasing, the water molecules can much more easily accelerate the exaltation of flexibility and mobility of their chain segment, that is able to induce their shape memory recovery in the water at room temperature. Therefore, the synergistic water-driven shape memory performance of the PVA/EP composite can be tailored by processing parameters and the ratio of PVA to EP.

3.4. Improving synergistic water-driven shape memory performance

The application fields of the PVA/EP composite can be expanded further by improving synergistic water-driven shape memory performance. As shown in Fig. S5, EP, PVA, and the PVA/EP composite surface are smooth without any pinholes or cracks. However, their surfaces are corroded after immersion in 10 wt% KOH solution for 8 h at 60 °C.

It is well known that the HCl, EtOH, and H_2O can be used as co-initiator polymerizing with Lewis acid. The co-initiator type and content have a significant effect on the reaction activity, that is, the suitable type and the reasonable ratio can accelerate its polymerization. Therefore, EP, PVA, and the PVA/EP composite are immersed in H_2O, HCl, EtOH, H_2O/EtOH, and HCl/EtOH solution for investigating their influence on the properties of the PVA/EP composite. The immersed EP, PVA, and the PVA/EP composite are designated as X-H_2O, X-HCl, X-EtOH, X-H_2O/EtOH, and X-HCl/EtOH, in which X represents EP, PVA, or the PVA/EP composite. There are EP-H_2O, EP-HCl, EP-EtOH, EP-H_2O/EtOH, EP-HCl/EtOH, PVA-H_2O, PVA-HCl, PVA-EtOH, PVA-H_2O/EtOH, PVA-HCl/EtOH, PVA/EP-H_2O, PVA/EP-HCl, PVA/EP-EtOH, PVA/EP-H_2O/EtOH, and PVA/EP-HCl/EtOH, respectively.

FTIR spectra of untreated and immersed EP, PVA, and the PVA/EP composite are shown in Fig. 6. The FTIR spectra show the PVA/EP-HCl/EtOH is much different with the PVA/EP composite. The absorption peaks at 1344 cm^{-1} and 1099 cm^{-1} are characteristic absorption peak of C—O. And the absorption peak at 959 cm^{-1} is attributed to the epoxy terminated group. It indicates that HCl/EtOH also can promote the chain termination of cationic polymerization which is difficult to stop in general. It's worth noting that the C—F absorption peak strength at 1181 cm^{-1} of PVA/EP-HCl/EtOH has a little increase that is attributed to F of PC and C of E-

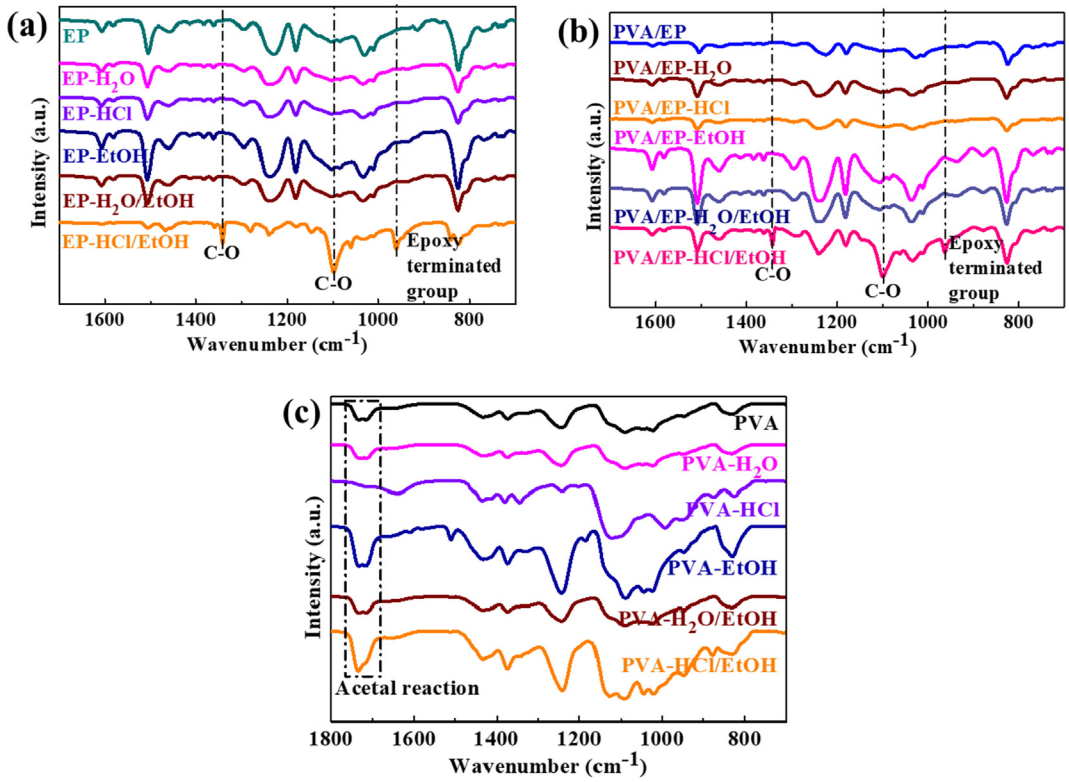

Fig. 6. FTIR spectra of EP (a), the PVA/EP composite (b), PVA (c): untreated and immersed in H_2O, HCl, EtOH, H_2O/EtOH, and HCl/EtOH.

51 forming more C-F in the HCl/EtOH solution compared with the PVA/EP composite. Furthermore, the epoxy group characteristic absorption peak (912 cm^{-1}) relative strength of EP and the PVA/EP composite immersed in HCl/EtOH are weaker than untreated EP and the PVA/EP composite, which suggest the epoxy monomers of the EP-HCl/EtOH and the PVA/EP-HCl/EtOH are rapidly consumed in HCl/EtOH solution. The absorption peaks at 1736 cm^{-1} and 1714 cm^{-1} are attributed to the acetal reaction between PVA and GA (Fig. 6(c)). These results indicate that 0.1 mol/L HCl/EtOH solution can be used as a suitable co-initiator for the PVA/EP composite. Comparing EP, PVA, the PVA/EP composite of untreated and immersed in H_2O, HCl, EtOH, H_2O/EtOH, and HCl/EtOH, these co-initiators are only useful for EP and the PVA/EP composite.

Penczek et al. proposes the activated monomer mechanism that the polymerization rate of epoxy monomers can be accelerated in the alcohol [39]. According to the activated monomer mechanism, the EtOH facilitates the protons exchange from the growth chain to the monomer resulting in generating new segments. Therefore, the epoxy monomer can be rapidly consumed to form much more hydrophilic groups in the PVA/EP-HCl/EtOH which can conducive to form hydrogen bonds with water molecules in humid environment improving its synergistic water-driven shape memory performance.

In consequence, the shape memory recovery process of EP-HCl/EtOH and PVA/EP-HCl/EtOH in the water and in the air at room temperature are shown in Fig. 7. The PVA/EP composite were immersed in 0.1 mol/L HCl/EtOH for 6 h, washed with deionized water, and dried at 60 °C for 12 h. After this post-treatment, the EP and PVA/EP composite are designated as EP-HCl/EtOH, PVA-HCl/EtOH, and PVA/EP-HCl/EtOH, respectively. It is also verified that the water is essential condition for inducing the shape memory recovery process of PVA/EP-HCl/EtOH at room temperature. Interestingly, the synergistic water-driven shape memory performance of the PVA/EP composite is improved after the post-treatment. It is obvious that the R_r of the PVA/EP-HCl/EtOH reaches 25% in the water only for 3 h. Compared with the PVA/EP composite, the PVA/EP-HCl/EtOH has recovered to 90° in water at room temperature within 12 h whose shape memory recovery speed is twice as fast. Five shape memory cycles are performed to examine durability of the PVA/EP-HCl/EtOH. The shape memory fixing ratios maintain above 95% in air at room temperature and the shape memory recovering ratios are above 93% in water at room temperature (Fig. S6). It is a surprise that the EP-HCl/EtOH still does not have water-driven shape memory ability at room temperature.

Although the water-driven shape memory performance of the PVA/EP composite is significantly improved by treating with 0.1 mol/L HCl/EtOH, the influence of HCl/EtOH on the PVA/EP composite is a problem worth considering. The results of SEM show that the HCl/EtOH solution does not damage the PVA/EP composite surface in Fig. 8.

The Fig. S7 is the high-resolution XPS spectra of the O1s region for EP-HCl/EtOH and PVA/EP-HCl/EtOH. The PVA/EP-HCl/EtOH can interact with water and show water-driven SME (Fig. 6 and Fig. 7), which also can be attributed to its abundant oxygen-containing functional groups especially for C-O-H compared with EP-HCl/EtOH. Therefore, the oxygen containing functional group is another influence factors on water-driven SME of the composites. These results are also corresponding to the analysis of FTIR spectra (Fig. 1 and Fig. 6).

It is worth noting that the T_g range of PVA/EP-HCl/EtOH is lower than the PVA/EP composite and there are two tan δ peak in the DMA thermograms of PVA/EP-HCl/EtOH, in Fig. 9 (a). It could be attributed to the intermolecular hydrogen bond of the composites further influenced by the HCl/EtOH solution. In addition, the curing rate and crosslinking density of the PVA/EP-HCl/EtOH have also changed. It is also suggested that shoulder peaks of the tan δ are attributed to the interaction effect of PVA chain segment and EP chain segment in the PVA/EP composite (Fig. 3 (e)). These results

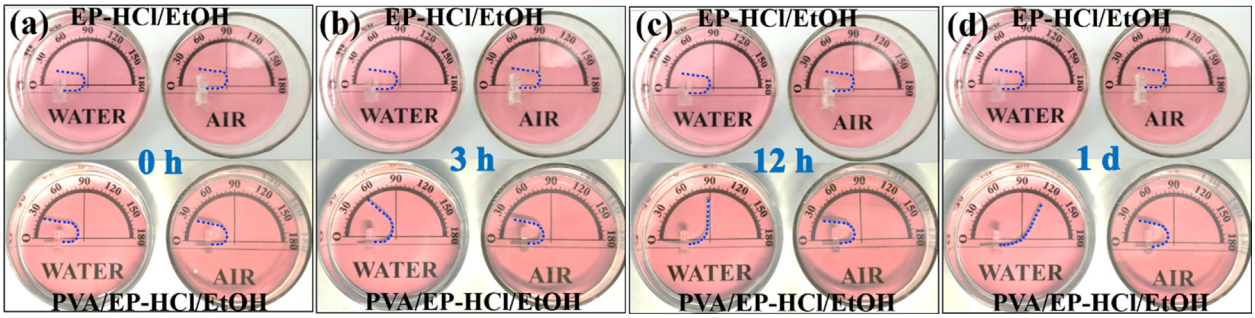

Fig. 7. Compared with shape memory recovery process of EP-HCl/EtOH and PVA/EP-HCl/EtOH in the water and in the air at room temperature. In each photograph: the top left corner one is EP-HCl/EtOH in water; the top right corner one is EP-HCl/EtOH in air; the lower left corner one is PVA/EP-HCl/EtOH in water; and the lower right corner one is PVA/EP-HCl/EtOH in air.

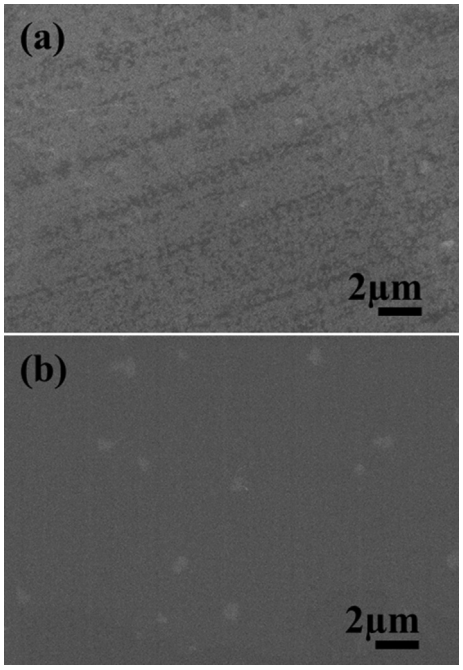

Fig. 8. SEM images of the PVA/EP composite (a) and PVA/EP-HCl/EtOH (b).

are also corresponding to the analysis of DSC curves (Fig. 3 (b)) and FTIR spectra (Fig. 6). In consequence, the T_g of the PVA/EP composites can be tailored by the post-treatment and the ratio of PVA to EP.

The E'_g of PVA/EP-HCl/EtOH is 3005.13 MPa at −6 °C and the E'_r of PVA/EP-HCl/EtOH is 4.68 MPa at 100.56 °C, so the value of E'_g/E'_r is about 650. In the Fig. 3 and Fig. 9, the loss modulus of PVA/EP-HCl/EtOH is higher than the PVA/EP composite at room temperature, however, the storage modulus and tensile strength of the PVA/EP composite becomes lower after immersed in HCl/EtOH solution at room temperature. The post-treatment, that the composite is immersed in the HCl/EtOH solution, is easy, efficient, economical strategy to improving synergistic water-driven shape memory performance as well as achieving applicable stiffness which is stiffer than PVA but softer than the PVA/EP composite at room temperature in Fig. 3 (d and f) and Fig. 9 (a). Like most of hydrophilic SMPs, the PVA has water-driven shape memory performance, but poor stiffness. The EP usually has stiffness and thermally-driven shape memory performance, but not water-driven shape memory recovering capacity. Therefore, the PVA/EP-HCl/EtOH is able to combine the virtues of both EP and PVA. After immersed in HCl/EtOH solution, the chain segments mobility and flexibility of the composite are improved, so that it is softer than the PVA/EP composite at room temperature. More than anything, PVA of the composite and the post-treatment with HCl/EtOH are major contributors to possess and improve its synergistic water-driven shape memory performance.

The underwater smart deployment and release structure is one of potential applications for the water-driven PVA/EP-HCl/EtOH. On the base of above study, Fig. 10 and Movie S1 (Supporting Information) exhibit the controllable underwater deployment and release process of a representative water-driven shape memory structure system. The pre-deformation PVA/EP-HCl/EtOH is assembled into a bud structure in which a dyed aerogel is wrapped. This water-driven shape memory structure system is fixed at container bottom, then it is immersed into the water. The wrapped green

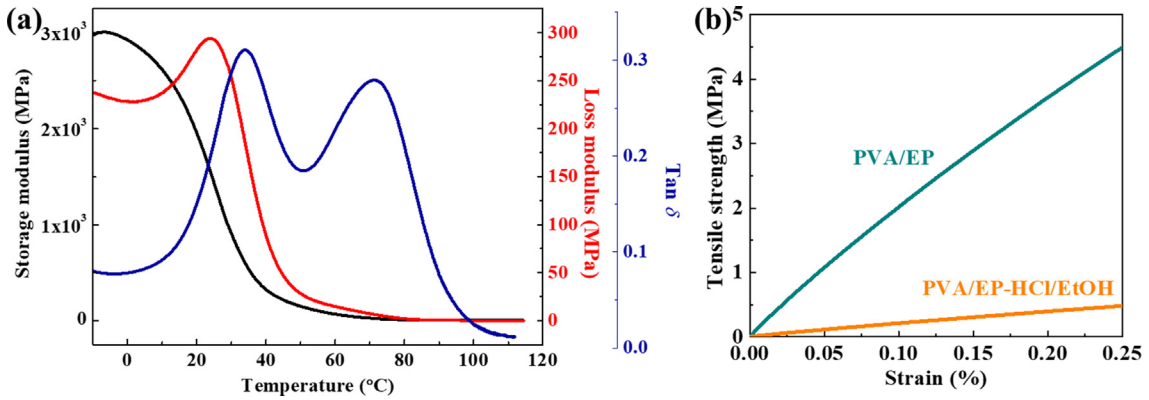

Fig. 9. DMA thermograms of PVA/EP-HCl/EtOH (a), Stress – strain curves of the PVA/EP composite and PVA/EP-HCl/EtOH (b).

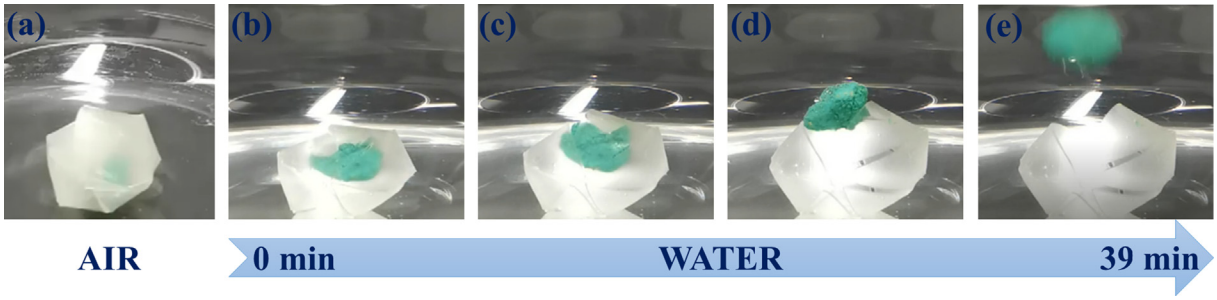

Fig. 10. A potential application demonstration of the PVA/EP-HCl/EtOH: the pre-deformation deployment and release structure is fixed at container bottom in air (a), the controllable underwater deployment and release process of a representative shape memory structure system in water (b ~ e).

aerogel is released with deployment of the water-driven PVA/EP-HCl/EtOH within 39 min. The advantage of this underwater smart deployment and release structure is attributed to the following points. First, the multi-stimuli responsive performance of PVA/EP-HCl/EtOH enable deform under thermal environment and fix after cooling. According to practical demands, it is able to deploy at a preset time and mode under water with recovering its initial shape and release process of the inside material. Also, the EP content of the composite could be adjusted to achieve applicable stiffness for performing protection, deployment, and release tasks of the inside material. Moreover, the water-driven shape memory recovering speed can be adjusted in a wide range by PVA content of the composite and/or the post-treatment with HCl/EtOH, in order to satisfy specific adsorption, catalysis, degradation, or detection task needs. Finally, this underwater smart deployment and release structure can stay at pre-set depth position via adjusting counterweight to achieve the deployment and release task at the different water depth.

From the foregoing, the performance of underwater shape memory deployment and release structure can be regulated and controlled by each component content, main technical parameter, pre-deformed condition, and deployed condition. Expectedly, this underwater smart deployment and release structure has flexible designability, workability, and low cost.

4. Conclusions

This work develops a grading photo-thermal curing PVA/EP composite with synergistic water-driven shape memory performance at a lower temperature condition. In the composite, the EP part is designed for maintaining applicable stiffness during water-driven shape memory recovery process, and the PVA part plays a critical role in triggering its water-driven SME. Interestingly enough, the synergistic plastifications, between hydroxyl groups of PVA, C-F of EP, other oxygen-containing functional groups in the PVA/EP composite, and the water molecules, are the main influence for its water-driven shape memory performance. As expected, the synergistic water-driven shape memory performance of the PVA/EP composite is improved after immersed in 0.1 mol/L HCl/EtOH for 6 h according to the activated monomer mechanism. One of potential applications for PVA/EP-HCl/EtOH is the underwater smart deployment and release structure. In conclusion, the performances of this composite and smart structure system with flexible designability and workability are able to be adjusted and customized by each component content and main technical parameter. It is noteworthy that the original fabrication and post-treatment strategy can be popularized to other smart composite and structure system, which could draw much attention due to various promising potential applications including marine resource utilization, deep-sea exploration, sensor, water purification, drug release, and flexible electronic devices.

Declaration of Competing Interest

The authors declare that they have no known competing financial interests or personal relationships that could have appeared to influence the work reported in this paper.

Acknowledgements

This work was supported by Hainan Provincial Natural Science Foundation of China (grant number 2019RC091; 520QN222); National Natural Science Foundation of China (grant numbers 11902105); Science Foundation of the National Key Laboratory of Science and Technology on Advanced Composites in Special Environments, China (grant numbers JCKYS2020603C012); Start-up Scientific Research Foundation of Hainan University, China (grant number KYQD(ZR)1813); Science Foundation of the State Key Laboratory of Marine Resource Utilization in South China Sea, China (grant numbers MRUKF2021037), for which we are very grateful.

Appendix A. Supplementary material

Supplementary data to this article can be found online at https://doi.org/10.1016/j.matdes.2022.110397.

References

[1] B. Zhang, H.G. Li, J.X. Cheng, H.T. Ye, A.H. Sakhaei, C. Yuan, P. Rao, Y.F. Zhang, Z. Chen, R. Wang, X.N. He, J. Liu, R. Xiao, S.X. Qu, Q. Ge, Mechanically robust and UV-curable shape-memory polymers for digital light processing based 4D printing, Adv. Mater. 33 (27) (2021) 2101298, https://doi.org/10.1002/adma.202101298.
[2] J.S. Leng, X. Lan, Y.J. Liu, S.Y. Du, Shape-memory polymers and their composites: stimulus methods and applications, Prog. Mater. Sci. 56 (7) (2011) 1077–1135, https://doi.org/10.1016/j.pmatsci.2011.03.001.
[3] W.X. Wang, Y.J. Liu, J.S. Leng, Recent developments in shape memory polymer nanocomposites: actuation methods and mechanisms, Coordin. Chem. Rev. 320–321 (2016) 38–52, https://doi.org/10.1016/j.ccr.2016.03.007.
[4] Y.L. Shao, J. Zhao, Y. Fan, Z.P. Wan, L.S. Lu, Z.H. Zhang, W.H. Ming, L.Q. Ren, Shape memory superhydrophobic surface with switchable transition between "lotus effect" to "rose petal effect", Chem. Eng. J. 382 (2020) 122989, https://doi.org/10.1016/j.cej.2019.122989.
[5] W.W. Liu, H.R. Chen, M.Q. Ge, Q.Q. Ni, Q. Gao, Electroactive shape memory composites with TiO_2 whiskers for switching an electrical circuit, Mater. Design 143 (2018) 196–203, https://doi.org/10.1016/j.matdes.2018.02.005.
[6] H.Z. Wu, P. Chen, C.Z. Yan, C. Cai, Y.S. Shi, Four-dimensional printing of a novel acrylate-based shape memory polymer using digital light processing, Mater. Design 171 (2019) 107704, https://doi.org/10.1016/j.matdes.2019.107704.
[7] A.K. Bastola, M. Hossain, The shape-morphing performance of magnetoactive soft materials, Mater. Design 211 (2021) 110172, https://doi.org/10.1016/j.matdes.2021.110172.
[8] W. Zhang, H. Wang, H.T. Wang, J.Y.E. Chan, H.L. Liu, B. Zhang, Y.F. Zhang, K. Agarwal, X.L. Yang, A.S. Ranganath, H.Y. Low, Q. Ge, J.K.W. Yang, Structural multi-colour invisible inks with submicron 4D printing of shape memory

polymers, Nat. Commun. 12 (2021) 112, https://doi.org/10.1038/s41467-020-20300-2.
[9] X.H. Cui, J.W. Chen, Y.T. Zhu, W. Jiang, Natural sunlight-actuated shape memory materials with reversible shape change and self-healing abilities based on carbon nanotubes filled conductive polymer composites, Chem. Eng. J. 382 (2020) 122823, https://doi.org/10.1016/j.cej.2019.122823.
[10] F. Guo, X.W. Zheng, C.Y. Liang, Z. Xu, Z.D. Jiao, Y.J. Liu, H.Y. Sun, L. Ma, W.W. Gao, A. Greiner, S. Agarwal, C. Gao, Millisecond response of shape memory polymer nanocomposite aerogel powered by stretchable graphene framework, ACS Nano 13 (5) (2019) 5549–5558, https://doi.org/10.1021/acsnano.9b00428.
[11] Y. Xie, Y. Meng, W.X. Wang, E. Zhang, J.S. Leng, Q.B. Pei, Bistable and reconfigurable photonic crystals-electroactive shape memory polymer nanocomposite for ink-free rewritable paper, Adv. Funct. Mater. 28 (34) (2018) 1802430, https://doi.org/10.1002/adfm.201802430.
[12] X. Zhang, C.Y. Zhu, B. Xu, L. Qin, J. Wei, Y.L. Yu, Rapid, localized and athermal shape memory performance triggered by photoswitchable glass transition temperature, ACS Appl. Mater. Inter. 11 (49) (2019) 46212–46218, https://doi.org/10.1021/acsami.9b17271.
[13] W.X. Wang, X.B. Liu, W. Xu, H.Q. Wei, Y.J. Liu, Y. Han, P. Jin, H.J. Du, J.S. Leng, Light-induced microfluidic chip based on shape memory gold nanoparticles/poly (vinyl alcohol) nanocomposites, Smart Mater. Struct. 27 (10) (2018) 105047, https://doi.org/10.1088/1361-665X/aadf6c.
[14] X.D. Qi, X.L. Yao, S. Deng, T.N. Zhou, Q. Fu, Water-induced shape memory effect of graphene oxide reinforced polyvinyl alcohol nanocomposites, J. Mater. Chem. A 2 (7) (2014) 2240–2249, https://doi.org/10.1039/C3TA14340F.
[15] W.X. Wang, H.B. Lu, Y.J. Liu, J.S. Leng, Sodium dodecyl sulfate/epoxy composite: water induced shape memory effect and its mechanism, J. Mater. Chem. A 2 (15) (2014) 5441–5449, https://doi.org/10.1039/C3TA15204A.
[16] T.Y. Fang, L.L. Cao, S.P. Chen, J.J. Fang, J. Zhou, L. Fang, C.H. Lu, Z.Z. Xu, Preparation and assembly of five photoresponsive polymers to achieve complex light-induced shape deformations, Mater. Design 144 (2018) 129–139, https://doi.org/10.1016/j.matdes.2018.02.029.
[17] D. Chen, X.H. Xia, T.W. Wong, H. Bai, M. Behl, Q. Zhao, A. Lendlein, T. Xie, Omnidirectional shape memory effect via lyophilization of PEG hydrogels, Macromol. Rapid Commun. 38 (7) (2017) 1600746, https://doi.org/10.1002/marc.201600746.
[18] W.X. Wang, L.W. Du, Y. Xie, F.H. Zhang, P. Li, F. Xie, X. Wan, Q.B. Pei, J.S. Leng, N. Wang, Bioinspired four-dimensional polymeric aerogel with programmable temporal-spatial multiscale structure and functionality, Compos. Sci. Technol. 206 (2021) 108677, https://doi.org/10.1016/j.compscitech.2021.108677.
[19] H.L. Gao, W.T. Dai, Y. Miao, Y.Z. Wang, D. Ma, W. Xue, Sustained heparin release actuator achieved from thermal and water activated shape memory hydrogels containing main-chain LC units, Chem. Eng. J. 339 (2018) 459–467, https://doi.org/10.1016/j.cej.2018.02.009.
[20] C. Yuan, F.F. Wang, B.Y. Qi, Z. Ding, D.W. Rosen, Q. Ge, 3D printing of multi-material composites with tunable shape memory behavior, Mater. Design 193 (2020) 108785, https://doi.org/10.1016/j.matdes.2020.108785.
[21] C.H. Zhou, Y.R. Ni, W.T. Liu, B. Tan, M.C. Yao, L. Fang, C.H. Lu, Z.Z. Xu, Near-infrared light-induced sequential shape recovery and separation of assembled temperature memory polymer microparticles, Macromol. Rapid Commun. 41 (8) (2020) 2000043, https://doi.org/10.1002/marc.202000043.
[22] A. Belmonte, M.P.D. Cunha, K. Nickmans, A.P.H.J. Schenning, Brush-paintable, temperature and light responsive triple shape-memory photonic coatings based on micrometer-sized cholesteric liquid crystal polymer particles, Adv. Opt. Mater. 8 (9) (2020) 2000054, https://doi.org/10.1002/adom.202000054.
[23] E.C. Davidson, A. Kotikian, S.C. Li, J. Aizenberg, J.A. Lewis, 3D printable and reconfigurable liquid crystal elastomers with light-induced shape memory via dynamic bond exchange, Adv. Mater. 32 (1) (2020) 1905682, https://doi.org/10.1002/adma.201905682.
[24] G. Stoychev, A. Kirillova, L. Ionov, Light-responsive shape-changing polymers, Adv. Opt. Mater. 7 (16) (2019) 1900067, https://doi.org/10.1002/adom.201900067.
[25] C.J. Huang, J.S. Peng, Y.R. Cheng, Q. Zhao, Y. Du, S.X. Dou, A.P. Tomsia, H.D. Wagner, L. Jiang, Q.F. Cheng, Ultratough nacre-inspired epoxy-graphene composites with shape memory properties, J. Mater. Chem. A 7 (6) (2019) 2787–2794, https://doi.org/10.1039/C8TA10725D.
[26] L. Sun, W.M. Huang, T.X. Wang, H.M. Chen, C. Renata, L.W. He, P. Lv, C.C. Wang, An overview of elastic polymeric shape memory materials for comfort fitting, Mater. Design 136 (2017) 238–248, https://doi.org/10.1016/j.matdes.2017.10.005.
[27] C.H. Linghu, S. Zhang, C.J. Wang, K.X. Yu, C.L. Li, Y.J. Zeng, H.D. Zhu, X.H. Jin, Z.Y. You, J.Z. Song, Universal SMP gripper with massive and selective capabilities for multiscaled, arbitrarily shaped objects, Sci. Adv. 6 (7) (2020) 5120, https://doi.org/10.1126/sciadv.aay5120.
[28] H.U. Rehman, Y.J. Chen, M.S. Hedenqvist, R. Pathan, H.Z. Liu, H.S. Wang, T. Chen, X.M. Zhang, H. Li, High-cycle-life and high-loading copolymer network with potential application as a soft actuator, Mater. Design 182 (2019) 108010, https://doi.org/10.1016/j.matdes.2019.108010.
[29] W.X. Wang, D.Y. Liu, Y.J. Liu, J.S. Leng, D. Bhattacharyya, Electrical actuation properties of reduced graphene oxide paper/epoxy-based shape memory composites, Compos. Sci. Technol. 106 (2015) 20–24, https://doi.org/10.1016/j.compscitech.2014.10.016.
[30] T. Sauter, K. Kratz, M. Heuchel, A. Lendleina, Fiber diameter as design parameter for tailoring the macroscopic, Mater. Design 202 (2021) 109546, https://doi.org/10.1016/j.matdes.2021.109546.
[31] A. Li, J.Z. Fan, G.Q. Li, Recyclable thermoset shape memory polymers with high stress and energy output via facile UV-curing, J. Mater. Chem. A 6 (24) (2018) 11479–11487, https://doi.org/10.1039/C8TA02644K.
[32] H. Okuzaki, T. Kuwabara, K. Funasaka, T. Saido, Humidity-sensitive polypyrrole films for electro-active polymer actuators, Adv. Funct. Mater. 23 (36) (2013) 4400–4407, https://doi.org/10.1002/adfm.201203883.
[33] W.M. Huang, B. Yang, L. An, C. Li, Y.S. Chan, Water-driven programmable polyurethane shape memory polymer: demonstration and mechanism, appl, Phys. Lett. 86 (11) (2005) 114105, https://doi.org/10.1063/1.1880448.
[34] Y.S. Wong, A.V. Salvekar, K.D. Zhuang, H. Liu, W.R. Birch, K.H. Tay, W.M. Huang, S.S. Venkatraman, Bioabsorbable radiopaque water-responsive shape memory embolization plug for temporary vascular occlusion, Biomaterials 102 (2016) 98–106, https://doi.org/10.1016/j.biomaterials.2016.06.014.
[35] C. Wang, Y.M. Zhang, J.M. Li, Z.H. Yang, Q.H. Wang, T.M. Wang, S. Li, S.B. Chen, X.R. Zhang, Shape memory properties of interpenetrating polymer networks (IPNs) based on hyperbranched polyurethane (HBPU), Eur. Polym. J. 123 (2020) 109393, https://doi.org/10.1016/j.eurpolymj.2019.109393.
[36] Z.Q. Fang, Y.D. Kuang, P.P. Zhou, S.Y. Ming, P.H. Zhu, Y. Liu, H.L. Ning, G. Chen, Programmable shape recovery process of water-responsive shape-memory poly(vinyl alcohol) by wettability contrast strategy, ACS Appl. Mater. Inter. 9 (6) (2017) 5495–5502, https://doi.org/10.1021/acsami.6b14868.
[37] H.X. Wan, J.X. Shen, N.S. Gao, J. Liu, Y.Y. Gao, L.Q. Zhang, Tailoring the mechanical properties by molecular integration of flexible and stiff polymer networks, Soft Matter 14 (12) (2018) 2379–2390, https://doi.org/10.1039/C7SM02282D.
[38] H.Y. Du, J.H. Zhang, Solvent induced shape recovery of shape memorypolymer based on chemically cross-linked poly(vinyl alcohol), Soft Matter 6 (14) (2010) 3370–3376, https://doi.org/10.1039/B922220K.
[39] K. Brzezinska, R. Szymanski, P. Kubisa, S. Penczek, Activated monomer mechanism in cationic polymerization, 1. ethylene oxide, formulation of mechanism, Macromol. Rapid Commun. 7 (1) (1986) 1–4, https://doi.org/10.1002/marc.1986.030070101.